galaxies

IMPACT FACTOR 3.8

CITESCORE 6.3

Article

On the Ionization Tolerance of C_{20} Fullerene in Ground and Excited Electronic States in Planetary Nebulae

SeyedAbdolreza Sadjadi and Quentin Andrew Parker

Special Issue

Origins and Models of Planetary Nebulae

Edited by

Dr. Andreas Ritter and Prof. Dr. Xuan Fang

MDPI

https://doi.org/10.3390/galaxies12060084

galaxies

MDPI

Article

On the Ionization Tolerance of C_{20} Fullerene in Ground and Excited Electronic States in Planetary Nebulae

SeyedAbdolreza Sadjadi *,†,‡ and Quentin Andrew Parker *,†,‡

Laboratory for Space Research, Faculty of Science, The University of Hong Kong, Hong Kong SAR, China
* Correspondence: ssadjadi@hku.hk (S.S.); quentinp@hku.hk (Q.A.P.)
† Current address: Room 405B, Block A, Cyberport 4, 100 Cyberport Road, Hong Kong Island, Hong Kong SAR, China
‡ These authors contributed equally to this work.

Abstract: As the smallest member of the fullerene family, C_{20} is yet to be discovered in planetary nebulae. In this work, we present a quantum chemical study via density functional theory (DFT) and partially by the MP2 on the ionization tolerance of this molecule in the space environment. Considering that the ionization and excitation phenomena play key roles in demonstrating the lifetime of a molecule, we examined both ground and excited electronic-state potential energy surfaces (PES) of C_{20} and its cations $C_{20}{}^{q+}$. Our theoretical results indicate that the C_{20} cage tolerates a positive charge as high as 13+ by characterizing local minimum geometries on both the abovementioned electronic states. The results are backed by characterizing both $C_{20}{}^{12+}$ and $C_{20}{}^{13+}$ as local minimum geometries at the MP2 level of computations. We also explored, theoretically and systematically, scenarios in which the electronic structure of neutral C_{20} is excited to very high spin multiplicity (beyond triplet state), and local minimum molecular geometries with cage structures are well characterized. We anticipate that such structural resistance to excitation and ionization delivers a prolonged lifetime necessary for the spectroscopic detection of this interesting molecule and its cations in space and potentially in planetary nebulae (PN).

Keywords: astrochemistry; C_{20} fullerene; ionization; excited state; DFT; MP2; planetary nebulae

Citation: Sadjadi, S.; Parker, Q.A. On the Ionization Tolerance of C_{20} Fullerene in Ground and Excited Electronic States in Planetary Nebulae. *Galaxies* **2024**, *12*, 84. https://doi.org/10.3390/galaxies12060084

Academic Editor: Francesco Calura

Received: 26 August 2024
Revised: 22 November 2024
Accepted: 27 November 2024
Published: 30 November 2024

1. Introduction

The formation of the smallest member of the fullerene family C_{20} (with 12 pentagon rings) in the gas phase was reported by Pinzach et al. in 2000 [1,2] via a chemo-synthetic procedure starting from $C_{20}H_{20}$, the fully hydrogenated form of C_{20}. Shortly after that, the synthesis of C_{20} in a solid state was achieved under laboratory conditions by Wang et al. [3] and Iqbal et al. [4]. Recently, Torrisi et al. [5] identified the formation of this species in the hot plasma (30 eV kinetic energy equivalent to Boltzmann's temperature of 348,100 K) of carbon atoms generated by a laser. This condition resembles the physical conditions at subsurface regions of central stars in planetary nebulae.

These interesting astronomical sources [6] are some of the sources of mysterious Unidentified Infrared Emission (UIE) bands attributed to the formation of complex organic molecules [7,8] including fullerenes [9,10] and fulleranes [11,12]. Although in terms of its chemical properties, such as molecular structure, chemical bonding, chemical reactivity, and lifetime, C_{20} fullerene is a focus for both theoretical [13] and experimental studies [14], in the astrochemistry of fullerenes in space, its status looks like a Darwinian lost species. Any knowledge of the stability of C_{20} (here, we mean the lifetime of a molecule in space before undergoing destruction by radiation) would not only significantly assist the efforts of detecting it but also create an understanding about the formation processes of other fullerenes, such as C_{60} and C_{70}, in astronomical sources [10]. The presence of C_{20} alongside other small members of the fullerene family, such as C_{24}

and C_{26}, has been speculated in planetary nebulae using theoretically calculated IR spectra [13,15]. A glance at the latest census of confirmed interstellar molecules [16] reveals that only a small number of pure carbon clusters, such as C_2 (at near Infrared), C_3 (at mid-Infrared), C_5 (at mid-Infrared), C_{60} (at mid-Infrared), C_{60}^+ (at mid-Infrared), and DIBs), and C_{70} (at mid-Infrared), have been detected. Other carbon clusters and members of the fullerene family, including C_{20}, are still to be found.

In comparison with C_{60}, with the positive heat of formation of 2520.0 ± 20.7 kJ·mol^{-1} [17], C_{20} fullerene also shows a positive heat of formation (2358.2 ± 8.0 kJ·mol^{-1} [18]; however, it is less positive than C_{60} by 161.8 kJ·mol^{-1}.

This delivers slightly more thermodynamic stability to C_{20}, which can potentially favor its formation in astronomical sources. Theoretically, the C_{20} fullerene shows high thermal stability in the gas and solid phases up to T = 3000 K before starting to convert to other isomers [19,20]. This is contrary to the existence of classical strain energy in this molecule [19]. This implies that such molecular species could survive in the outer regions of PN envelopes where the central-star UV radiation field is diminished and where dust and other molecular species in the form of globules and condensation can act as a shade mechanism. In the context of electronic structure, it was found that C_{60} fullerene shows an exceptional characteristic for rearrangement of its electron density that has led to the survival of a network of chemical bonds between carbon atoms at a high degree of ionization [21]. In laboratory conditions and theoretical calculations, C_{60} cations with a positive charge of as high as +12 [22] and +26 [21] have been reported, respectively. In the case of C_{20}, we anticipate qualitatively lower tolerance toward ionization and excitation. However, we also look at scenarios where C_{20} undergoes a low, moderate, and high degree of electronic excitation without ionization. In this way, we explore the structural stability of this molecule under the extremely high electronic multiplicity. A comprehensive report on the high thermal and mechanical stabilities and other interesting molecular properties, such as superconductivity of neutral C_{20}, was published by Fei Lin et al. [23]. Considering all these backgrounds, the present work aims to examine molecular structure responses of C_{20} to extreme radiation conditions of planetary nebulae via first-principle methods of quantum chemistry.

2. Quantum Chemical Computations

In this study, three series of systematic quantum chemical computations have been conducted on C_{20} fullerene (12 pentagons) and its cations within the density functional theory (DFT) framework [24,25]. In all computations, molecular geometries were optimized, and stationary points located on the potential energy surfaces were characterized by subsequent calculations of the Hessian matrix (second derivative of energy function). The B3LYP hybrid functional [26–28], which utilizes the VWN5 correlation functional [28,29], in part was applied in the restricted (R), unrestricted (U), and RO (Restricted open-shell) frameworks for singlet and higher electronic multiplicities, respectively. The polarization-consistent basis set (PC1) [30–32], which contains S, P, and D-type basis functions for carbon atoms, was integrated into the B3LYP framework. The first series of computations were conducted to create an understanding of the ionization tolerance of C_{20}. The general formula of species involved in this series is $C_{20}{}^{q+}$ $q = 0 - 14$. Singlet and doublet electronic multiplicities were set for species with even and odd values for q, respectively. The second series of computations was performed on the electronic excitation of local minimum geometries found in the first series to their next higher multiplicity. Species at singlet and doublet electronic states were studied at triplet and quartet excited states separately. The third series of computations were carried out on neutral C_{20} and at excited electronic states associated with the multiplicity of 3 to 21 (2–20 unpaired electrons). To support our DFT results, the computationally expensive ab initio correlated method MP2(FC) calculations combined with the same basis set family PC 1 were conducted on three species C_{20} (singlet), $C_{20}{}^{12+}$(singlet), and $C_{20}{}^{13+}$(doublet). MP2(FC) stands for the Møller–Plesset second-order perturbation theory and with frozen core (FC) approximation, in which only correla-

tion energy of valence electrons is treated by the theory. Singlet and doublet electronic states were treated by R and RO methodologies, respectively. All DFT and MP2(FC) electronic structure computations in this work have been performed using PC-GAMESS 8.2.0 (known as Firefly) Quantum Chemistry (QC) package [33] and without imposing symmetry constraint on geometry optimization. The Firefly QC package is partially based on the GAMESS (US) [34] source code. GAMESS stands for General Atomic and Molecular Electronic Structure System. ROMP2(FC) computations were performed by GAMESS (US) [34]. To explore the network of chemical bonding, the electron densities of all local minimum geometries were then analyzed within the framework of the Quantum Theory of Atoms in Molecules (QTAIM). The AIMALL package [35] was utilized for this purpose.

3. Discussion

3.1. Ionization Tolerance and Electronic Excitation

We have reported previously that the C_{60} fullerene ionization tolerance limit (ITL) stands at a charge of +26 [21]. With one third of the number of carbon atoms, one may estimate the ITL limit for C_{20} as +8 or +9. The results of our quantum chemical calculations (at the same level that was applied to C_{60}) combined with chemical-bonding analysis reveal that this limit stands at +13 for C_{20}. No stationary point on the Potential Energy Surface (PES) of C_{20}^{14+} at the singlet spin state was found. In other words, computational quantum chemistry calculation predicts that C_{20}^{14+} cannot be formed. Similar to C_{60}, the total electron density in C_{20} fullerene also shows a remarkable ability to redistribute itself to prevent the disintegration of the molecule at highly positively charged states. In Table 1, electronic multiplicity, dipole moments, and lowest harmonic vibrational frequency of all C_{20}^{q+} (local minimum geometries) are listed. Our MP2 computations presented in this table also confirm the formation of highly positively charged cations (+12 and +13) of C_{20}. The chemical-bonding analysis via QTAIM confirms that the network of bonding between carbon atoms and, thus, the cage structure of the molecule is well preserved for all highly positively charged C_{20} cations (Figure 1). We use the amount of the total electron density at the specific locations within the molecule to explore quantitatively the changes that occur upon ionization. These locations are marked by the formation of specific critical points (bond critical points—BCPs)that show how neighboring atoms are interacting with each other individually, which group of interacting atoms are forming a ring (ring critical point—RCP), and finally, if a group of the rings can form a cage structure (cage critical point—CCP)) (Figure 1). Our calculated values of electron density at these locations show that during the ionization process from C_{20} to C_{20}^{13+}, the electron density at the pentagon rings decreases by 40% on average (0.02 amu/0.05 amu, where amu is atomic mass unit). This value stands at around 50% (0.0028 amu/0.0053 amu) when calculated at the cage critical point. This remarkable ability of electron density to maintain the network of bonding and cage structure at the condition of electron density deficiency underlies the high ionization tolerance. It is anticipated that this characteristic is shown by other members of the fullerene family with different sizes. Considering this common behavior, their contribution to carrying elemental carbon to different locations in space would significantly increase. This will lead us to estimate the fractions of carbon mass produced in PNs and deposited in each of the allotropic forms (graphite, diamond, fullerene, and nanotube) in addition to atomic, diatomic, and carbon clusters. Each of these species may be a starting reactant for a certain class of astrochemical reaction(s) (or chain of reactions) and, therefore, molecular products (some perhaps are bio-molecules) with specific stereochemistry (for instance, cyclic, chain, optically active). Since the synthesis of all-metal fullerene (in the form of the inorganic complex made of Sb and Au) has been reported recently [36], it is an open question if any privileges have been naturally given to such molecular geometry for carrying the other elements throughout the universe.

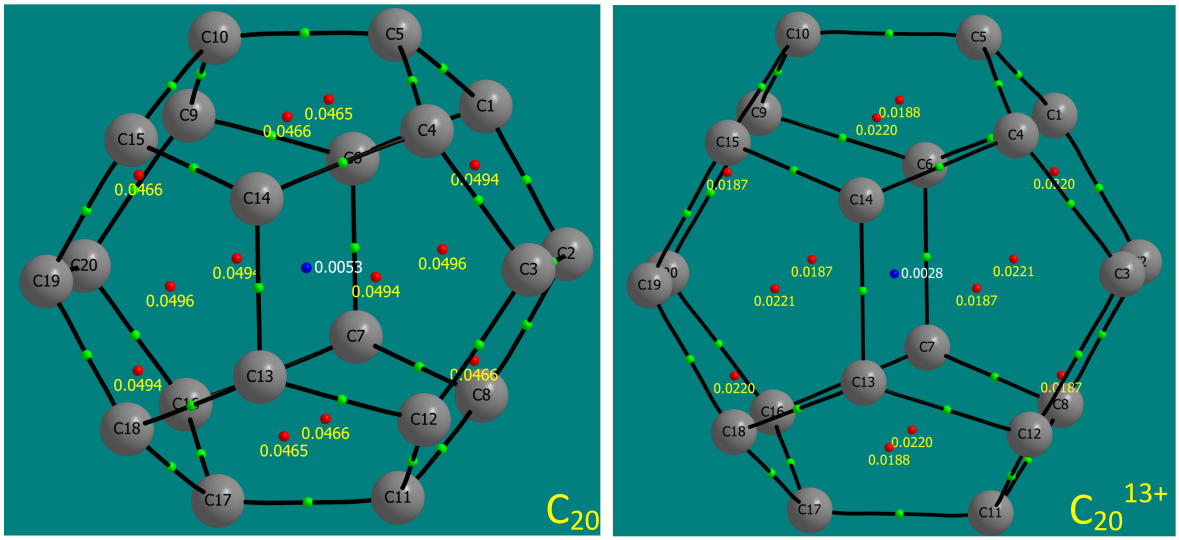

Figure 1. Molecular graphs representing bonding, structure, and amount of electron density for C_{20} and C_{20}^{13+} local minimum geometries at singlet and doublet electronic states, respectively. Color codes are carbon nuclei in gray circles, bond paths in solid black lines, bond critical points (BCP) in green circles, ring critical points (RCP) in red circles, cage critical points (CCP) in blue circles, and amount of electron density (in amu unit) at each RCP and CCP in yellow and white numbers separately. The quantum chemical model is B3LYP/PC1.

Table 1. Calculated molecular properties of C_{20}^{q+} species at B3LYP/PC1 level on local minimum geometries. All geometries uniformly possess C_i point group symmetry. MP2(FC)/PC1 and ROMP2(FC)/PC1 data (bold-italic font) are presented for C_{20}, C_{20}^{12+} and C_{20}^{13+}.

Species	Electronic Multiplicity	Dipole Moment (Debye)	Lowest Unscaled Frequency (cm^{-1})
C_{20}	1 (s) [1]	0.000319	158.33
C_{20}	***1***	***0.000118***	***379.07***
C_{20}^{+}	2 (d) [1]	0.000126	175.23
C_{20}^{2+}	1	0.001072	526.73
C_{20}^{3+}	2	0.000679	373.11
C_{20}^{4+}	1	0.001060	448.18
C_{20}^{5+}	2	0.000092	215.31
C_{20}^{6+}	1	0.000107	216.82
C_{20}^{7+}	2	0.000318	320.59
C_{20}^{8+}	1	0.000697	90.43
C_{20}^{9+}	2	0.000588	283.19
C_{20}^{10+}	1	0.000186	326.28
C_{20}^{11+}	2	0.000230	311.93
C_{20}^{12+}	1	0.000130	324.16
C_{20}^{12+}	***1***	***0.000042***	***320.59***
C_{20}^{13+}	2	0.000527	80.99
C_{20}^{13+}	***2***	***0.003384***	***240.6***

[1] (s) and (d) stand for singlet and doublet electronic states, respectively.

To confirm theoretically the assumed electronic multiplicities as the electronic ground states for C_{20}^{q+} species listed in Table 1, we conducted a series of computations on the next upper electronic multiplicity state. These data are presented in Table 2. All species in Table 2 are characterized as the local minimum geometries at their corresponding electronic states. Cage structure is maintained for all these species as determined by QTAIM calculations. We observed energy crossover between the Potential Energy Surface (PES) of single-triplet and doublet-quartet states for C_{20}^{q+} (q = 4–10). The crossover is between 1 and 8 kcal/mol

in favor of higher multiplicity states, i.e., triplet and quartet. We have combined the data in Tables 1 and 2 to calculate the energetics of step-wise ionization of C_{20}. The calculated step-wise ionization potentials (IPs) corrected to zero-point energy and their correspondence spectral region wavelengths and electronic states are presented in Table 3. Similar to the trend reported for C_{60} IP values (7.80–82.44 eV) [21], C_{20} values also cover the range between 7.35 and 65.99 eV. This demonstrates that this smallest member of the carbon fullerene family also has a chance to survive vacuum and extreme UV conditions. The last entry of Table 3 is the step-wise ionization potential of C_{20}^{12+} at the MP2 level of calculations. The difference between DFT and MP2 values is reported as 0.31 eV, equivalent to 0.09 nm in wavelength.

Table 2. Calculated molecular properties of C_{20}^{q+} species at B3LYP/PC1 level at local minimum geometries on high electronic multiplicity PES. All geometries uniformly possess C_i point group symmetry.

Species	Electronic Multiplicity	Dipole Moment (Debye)	Lowest Unscaled Frequency (cm^{-1})	Energy Difference to Lower Multiplicity State (kcal/mol) [1]
C_{20}	3 (t) [2]	0.000152	254.56	2.64
C_{20}^{+}	4 (qr) [2]	0.000937	299.29	40.59
C_{20}^{2+}	3	0.000353	396.04	39.98
C_{20}^{3+}	4	0.000734	311.31	31.01
C_{20}^{4+}	3	0.000073	311.46	−2.05
C_{20}^{5+}	4	0.000161	333.78	−3.32
C_{20}^{6+}	3	0.000269	160.93	−1.61
C_{20}^{7+}	4	0.000815	215.47	−2.46
C_{20}^{8+}	3	0.000185	227.84	−1.47
C_{20}^{9+}	4	0.000294	316.46	−7.68
C_{20}^{10+}	3	0.000469	247.25	−1.34
C_{20}^{11+}	4	0.000393	226.00	35.94
C_{20}^{12+}	3	0.000199	200.39	36.28
C_{20}^{13+}	4	0.000118	151.37	26.27

[1] Zero-point energy corrected values and with respect to Table 1 entries. [2] (t) and (qr) stands for triplet and quartet electronic state, respectively.

Table 3. Energetics of step-wise ionization that lead to C_{20}^{q+} species calculated at B3LYP/PC1 level on local minimum geometries [1]. All geometries uniformly possess C_i point group symmetry. Ionization potential of C_{20}^{12+} at MP2(FC) level is in bold-italic.

Step	Electronic Multiplicity	IP (eV) [2]	λ (nm)	Spectrum Region
$C_{20} \rightarrow C_{20}^{+}$	s→d	7.34 [3]	168.98	vacuum uv
$C_{20}^{+} \rightarrow C_{20}^{2+}$	d→s	12.02	103.13	vacuum uv
$C_{20}^{2+} \rightarrow C_{20}^{3+}$	s→d	18.88	65.66	extreme uv
$C_{20}^{3+} \rightarrow C_{20}^{4+}$	d→t	23.55	52.64	extreme uv
$C_{20}^{3+} \rightarrow C_{20}^{4+}$	d→s	23.64	52.44	extreme uv
$C_{20}^{4+} \rightarrow C_{20}^{5+}$	t→qr	28.45	43.59	extreme uv
$C_{20}^{4+} \rightarrow C_{20}^{5+}$	s→d	28.50	43.50	extreme uv
$C_{20}^{5+} \rightarrow C_{20}^{6+}$	qr→t	33.42	37.10	extreme uv
$C_{20}^{5+} \rightarrow C_{20}^{6+}$	d→s	33.34	37.19	extreme uv
$C_{20}^{6+} \rightarrow C_{20}^{7+}$	t→qr	38.05	32.59	extreme uv
$C_{20}^{6+} \rightarrow C_{20}^{7+}$	s→d	38.08	32.55	extreme uv
$C_{20}^{7+} \rightarrow C_{20}^{8+}$	qr→t	42.94	28.88	extreme uv
$C_{20}^{7+} \rightarrow C_{20}^{8+}$	d→s	42.89	28.91	extreme uv
$C_{20}^{8+} \rightarrow C_{20}^{9+}$	t→qr	47.23	26.55	extreme uv
$C_{20}^{8+} \rightarrow C_{20}^{9+}$	s→d	47.50	26.10	extreme uv
$C_{20}^{9+} \rightarrow C_{20}^{10+}$	qr→t	52.31	23.70	extreme uv
$C_{20}^{9+} \rightarrow C_{20}^{10+}$	d→s	52.03	23.83	extreme uv

Table 3. *Cont.*

Step	Electronic Multiplicity	IP (eV) [2]	λ (nm)	Spectrum Region
$C_{20}^{10+} \rightarrow C_{20}^{11+}$	t→d	56.54	21.93	extreme uv
$C_{20}^{10+} \rightarrow C_{20}^{11+}$	s→d	56.48	21.95	extreme uv
$C_{20}^{11+} \rightarrow C_{20}^{12+}$	d→s	60.52	20.49	extreme uv
$C_{20}^{12+} \rightarrow C_{20}^{13+}$	s→d	65.99	18.79	extreme uv
$\boldsymbol{C_{20}^{12+} \rightarrow C_{20}^{13+}}$	***s→d***	***66.30***	***18.70***	***extreme uv***

[1] Lower energy electronic multiplicity for C_{20}^{q+} $q = 4 - 10$ are also added to this table. [2] Zero-point energy corrected values. [3] 7.5 eV, DFT results [14].

3.2. Higher Electronic Multiplicity

High spin states are common phenomena among inorganic molecular clusters such as transition metals. Here, we conducted quantum mechanical calculations for the scenario that led to the electronic states on a neutral C_{20} with more than two unpaired electrons (triplet states). In this way, information on the responses of this molecule in abnormally high excitation states is explored. The argument may have arisen that such states have extremely short lifetimes, and the molecule may undergo disintegration before reaching such states. However, because molecular species are subject to unknown and often extreme conditions in the space environment that can range from low to high levels of temperature, pressure, radiation, density, electric and magnetic fields, etc., the opposite effects can be expected. This is like what we observe for the stability of very reactive species such as C_2 in space. Table 4 presents the results of the theoretical calculations on ultra-high spin electronic states of C_{20}. The QTAIM calculations confirm that all local minimum geometries found from the spin multiplicity of 3 to 17 (corresponding to 2–16 unpaired electrons) possess the cage structure as C_{20} (singlet). At the spin multiplicity of 19, the 12-pentagon structure turns into a 10-pentagon structure with 2 opened/elongated pentagons connected by a long-range weak bonding interaction between two carbon atoms C11–C17 (Figure 2). At a multiplicity of 21 (20 unpaired electrons), the bonding between C11 and C17 is ruptured, and as a result, the structure changes into the opened cage with 10 pentagon rings (Figure 2). Despite the significant differences in the spin multiplicity across the species in Table 4, the electron density values at RCPs and CCPs shown in Figure 2 are comparable. Energetics of such processes are listed in Table 4. Their values are comparable to the ionization energies listed in Table 3. This means that the two processes of ionization and excitation are competing with each other within the energy range of 8–23 eV. For instance, according to our theoretical values in Tables 3 and 4, a photon of 7.38 eV can lead to the ionization of one electron or with slightly higher energy at 8.14 eV to an ultra-high spin C_{20}.

Table 4. Calculated molecular properties of neutral C_{20} fullerene species at B3LYP/PC1 level at local minimum geometries on high electronic multiplicity PES.

Species	Unpaired Electrons	Electronic Multiplicity	PG [1]	Dipole Moment (Debye)	Lowest Unscaled Frequency (cm^{-1})	Energy Difference to Singlet State (kcal/mol) [2]	Energy Difference to Singlet State (eV) [2]
C_{20}	4	5	C_i	0.000256	286.57	37.87	1.64
	6	7	C_i	0.000023	303.66	83.29	3.61
	8	9	C_i	0.000681	311.33	137.86	5.98
	10	11	C_1	0.137266	94.47	187.80	8.14
	12	13	C_2	0.006378	332.16	237.11	10.28
	14	15	C_s	0.245907	185.37	344.60	14.94
	16	17	C_2	0.792567	290.08	452.92	19.64
	18	19	C_s	0.591260	228.76	521.17	22.60

[1] Symmetry point group. [2] Zero-point energy corrected values.

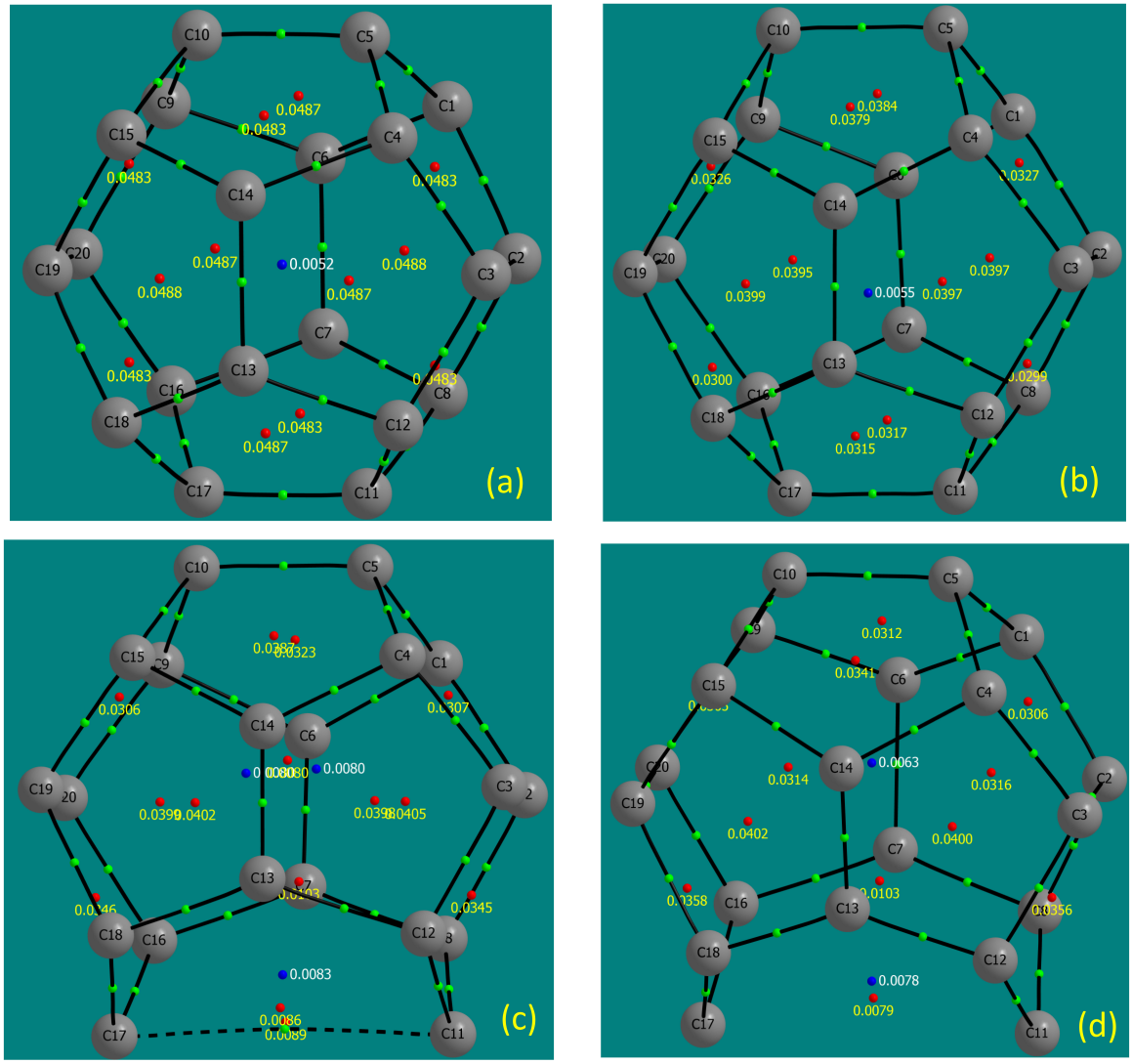

Figure 2. Molecular graphs representing bonding, structure and amount of electron density for C_{20} local minimum geometries at (**a**) triplet (**b**) spin multiplicity of 17 (**c**) spin multiplicity of 19 and (**d**) multiplicity of 21, respectively. Color codes are carbon nuclei in gray circles, bond paths in solid black line, weak bonding interaction in dashed solid black line, bond critical points (BCP) in green circles, ring critical points (RCP) in red circles, cage critical points (CCP) in blue circle, amount of electron density (in amu unit) at each RCP and CCP in yellow and white numbers separately. The quantum chemical model is B3LYP/PC1.

4. Conclusions

The C_{20} fullerene with its 12-pentagon structure shows a significant tolerance against disintegration upon ionization as well as excitation to high spin states. This is underpinning its abnormal thermal stability [23]. Cage structure is preserved in cationic forms in both the ground and excited potential energy surfaces and up to the charge limit of $q = +13$. Our DFT results are supported by calculations performed at the MP2 correlated level. In both cationic and radical forms, we found a few cases in which the molecule adopts the dipole moment to be detected by its rotation spectroscopic signature. With its ease of formation in the solid state reported in laboratory conditions and the stability of its electronic structure, we anticipate the detection of this smallest member of the fullerene family and its radical or cationic forms in the physical conditions present in planetary nebulae. Our study of changes in molecular bonding and structure at ultra-high spin conditions shows that only a few chemical bonds are broken in C_{20} at electronic multiplicity higher than 17 (16 unpaired electrons). This gives an extra chance of surviving to C_{20} in the harsh thermal, turbulence,

and radiation conditions in planetary nebulae. The results of our modeling encourage the search for this important and interesting molecule in astrophysical objects. We anticipate that sources are known to have C_{60} fullerene and are the primary targets for observation and detection of C_{20} and its cations. Based on our theoretical results, the lack of large dipole moments among most of these species suggests that infrared spectroscopy is the main means to detect these fullerenes. However, some of the polar geometries may be detectable via their rotational energy signatures (Rotational constants available in supplementary materials, Table S1). Theoretically calculated IR spectra of all the species in this work will be available from us in a subsequent publication.

Supplementary Materials: The following supporting information can be downloaded at: https://www.mdpi.com/article/10.3390/galaxies12060084/s1, Table S1: DFT calculated rotational constants of $C_{20}{}^{q+}$ $q = 1 - 13$

Author Contributions: S.S. has performed the computations. S.S. and Q.A.P. analyzed data and wrote the manuscript. All authors have read and agreed to the published version of the manuscript.

Funding: Q.A.P. and S.S. thanks the Hong Kong Research Grants Council for GRF research support under grants 17326116 and 17300417. S.S. would like to acknowledge the support of HKU Supercomputer facilities and the QuantumCube computer cluster of the Laboratory for Space Research (LSR). This article/publication is based upon work from COST Action CA21126-Carbon molecular nanostructures in space (NanoSpace), supported by COST (European Cooperation in Science and Technology.

Data Availability Statement: Data are contained within the article and supplementary materials

Conflicts of Interest: The authors declare no conflicts of interest.The funders had no role in the design of the study; in the collection, analyses, or interpretation of data; in the writing of the manuscript, or in the decision to publish the results

References

1. Pinzbach, H.; Weiler, A.; Landenberger, P.; Wahl, F.; Wörth, J.; Scott, L.T.; Gelmont, M.; Olevano, D.; Issendorff, B.V. Gas-phase production and photoelectron spectroscopy of the smallest fullerene, C_{20}. *Nature* **2000**, *407*, 60–63. [CrossRef] [PubMed]
2. Jarrold, M.F. The smallest fullerene. *Nature* **2000**, *407*, 26–27. [CrossRef] [PubMed]
3. Wang, Z.; Ke, X.; Zhu, Z.; Zhu, F.; Ruan, M.; Chen, H.; Huang, R.; Zheng, L. A new carbon solid made of the world's smallest caged fullerene C_{20}. *Phys. Lett. A* **2001**, *280*, 351–356. [CrossRef]
4. Iqbal, Z.; Zhang, Y.; Grebel, H.; Vijayalakshmi, S.; Lahamer, A.; Benedek, G.; Bernasconi, M.; Cariboni, J.; Spagnolatti, I.; Sharma, R.; et al. Evidence for a solid phase of dodecahedral C_{20}. *Eur. Phys. J. B* **2003**, *31*, 509–515. [CrossRef]
5. Torrisi, L.; Torrisi, A.; Cutroneo, M. Fullerene C_{20} carbon nucleation induced by IR ns pulsed laser-generated plasma. *Fuller. Nanotub. Carbon Nanostruct.* **2024**, *32*, 783–790.
6. Parker, Q.A.; Bojicic, I.S.; Frew, D. HASH: The Hong Kong/AAO/Strasbourg Hα planetary nebula database. *J. Phys. Conf. Ser.* **2016**, *728*, 032008. [CrossRef]
7. Kwok, S. The mystery of unidentified infrared emission bands. *Astrophys. Space Sci.* **2022**, *367*, 16. [CrossRef]
8. Cataldo, F.; García-Hernández, D.A.; Manchado, A. Petroleum, coal and other organics in space. *Astrophys. Space Sci.* **2020**, *365*, 81. [CrossRef]
9. Wood, P. The discovery of cosmic fullerenes. *Nat. Astron.* **2020**, *4*, 299–305. [CrossRef]
10. Cami, J.; Bernard-Salas, J.; Peeters, E.; Malek, S.E. Detection of C_{60} and C_{70} in a Young Planetary Nebula. *Science* **2010**, *329*, 1180–1182. [CrossRef]
11. Zhang, Y.; Sadjadi, S.A.; Hsia, C.-H. Hydrogenated fullerenes (fulleranes) in space. *Astrophys. Space Sci.* **2020**, *365*, 67. [CrossRef]
12. Diaz-Luis, J.J. A search for hydrogenated fullerenes in fullerene-containing planetary nebulae. *J. Phys. Conf. Ser.* **2016**, *728*, 052005. [CrossRef]
13. Adjizian, J.J.; Vlandas, A.; Rio, J.; Charlier, J.C.; Ewels, C.P. Ab initio infrared vibrational modes for neutral and charged small fullerenes (C_{20}, C_{24}, C_{26}, C_{28}, C_{30} and C_{60}). *Phil. Trans. R. Soc. A* **2016**, *374*, 201550323. [CrossRef] [PubMed]
14. Castro, A.; Marques, M.A.; Alonso, J.A.; Bertsch, G.F.; Yabana, K.; Rubio, A. Can optical spectroscopy directly elucidate the ground state of C_{20}? *J. Chem. Phys.* **2002**, *116*, 1930–1933. [CrossRef]
15. Sadjadi, S.; Kwok, S.; Cataldo, F.; García-Hernández, D.A.; Manchado, A. A theoretical investigation of the possible detection of C24 in space. *Fuller. Nanotub. Carbon Nanostruct.* **2020**, *28*, 637–641. [CrossRef]
16. McGuire, B.A. 2021 Census of Interstellar, Circumstellar, Extragalactic, Protoplanetary Disk, and Exoplanetary Molecules. *Astrophys. J. Suppl. Ser.* **2022**, *29*, 30. [CrossRef]

17. Chan, B.; Kawashima, Y.; Katouda, M.; Nakajima, T.; Hirao, K. From C_{60} to Infinity: Large-Scale Quantum Chemistry Calculations of the Heats of Formation of Higher Fullerenes. *J. Am. Chem. Soc.* **2016**, *138*, 1420–1429. [CrossRef]
18. Chan, B. Fullerene Thermochemical Stability: Accurate Heats of Formation for Small Fullerenes, the Importance of Structural Deformation on Reactivity, and the Special Stability of C_{60}. *J. Phys. Chem. A* **2020**, *124*, 6688–6698. [CrossRef]
19. Marcos, P.A. Simulating the thermal stability and phase changes of small carbon clusters and fullerenes. *Eur. Phys. J. D* **1999**, *6*, 221–233. [CrossRef]
20. Davydov, I.V.; Podlivaev, A.I.; Openov, L.A. Anomalous thermal stability of metastable C_{20} fullerene. *Phys. Solid State* **2005**, *47*, 778–784. [CrossRef]
21. Sadjadi, S.A.; Parker, Q.A. It remains a cage: Ionization tolerance of C_{60} fullerene in planetary nublae. *Fuller. Nanotub. Carbon Nanostruct.* **2021**, *29*, 620–625. [CrossRef]
22. Bhardwaj, V.R.; Corkum, P.B.; Rayner, D.M. Internal Laser-Induced Dipole Force at Work in C_{60} molecule. *Phys. Rev. Lett.* **2003**, *91*, 203004. [CrossRef] [PubMed]
23. Lin, F.; Sorensen, E.S.; Kallin, C.; Belinsky, A.J. C_{20}, the Smallest Fullerene. In *Handbook of Nanophysics: Clusters and Fullerenes*; Sattler, K.D., Ed.; Publishing House: Boka Raton, FL, USA, 2010; pp. 552–563.
24. Parr, R.G.; Yang, W. *Density Functional Theory of Atoms and Molecules*; Oxford University Press: New York, NY, USA 1989
25. Zigler, T. Approximate density functional theory as a practical tool in molecular energetics and dynamics. *Chem. Rev.* **1991**, *91*, 651–667 [CrossRef]
26. Beke, A.D. Density-functional thermochemistry. III. The role of exact exchange. *J. Chem. Phys.* **1993**, *98*, 5648–5652. [CrossRef]
27. Stephens, P.J.; Devlin, F.J.; Chabalowski, C.F.; Frisch, M.J. Ab initio Calculation of Vibrational Absorption and Circular Dichroism Spectra Using Density Functional Force Fields. *J. Phys. Chem.* **1994**, *98*, 11623–11627. [CrossRef]
28. Hertwig, R.H.; Koch, W. On the parameterization of the local correlation functional. What is Becke-3-LYP? *Chem. Phys. Lett.* **1997**, *268*, 345–351. [CrossRef]
29. Vosko, S.H.; Wilk, L.; Nusair, M. Accurate spin-dependent electron liquid correlation energies for local spin density calculations: A critical analysis. *Can. J. Phys.* **1980**, *58*, 1200–1211. [CrossRef]
30. Jensen, F. Polarization consistent basis sets: Principles. *J. Chem. Phys.* **2001**, *115*, 9113. [CrossRef]
31. Jensen, F. Polarization consistent basis sets. II. Estimating the Kohn-Sham basis set limit. *J. Chem. Phys.* **2002**, *116*, 7372. [CrossRef]
32. Jensen, F. Polarization consistent basis sets. III. The importance of diffuse functions. *J. Chem. Phys.* **2002**, *117*, 9234. [CrossRef]
33. Granovsky, A.A. Firefly Version 8.2.0. Available online: http://classic.chem.msu.su/gran/firefly/index.html (accessed on 30 December 2016).
34. Schmidt, M.W.; Baldridge, K.K.; Boatz, J.A.; Elbert, S.T.; Gordon, M.S.; Jensen, J.H.; Koseki, S.; Matsunaga, N.; Nguyen, K.A.; Su, S.; et al. General atomic and molecular electronic structure system. *J. Comput. Chem.* **1993**, *14*, 1347–1363. [CrossRef]
35. Keith, T.A. TK Gristmill Software. Available online: https://aim.tkgristmill.com/ (accessed 30 Decmber 2019).
36. Xu, Y.-H.; Tian, W.-J.; Muñoz-Castro, A.; Frenking, G.; Sun, Z.-M. An all-metal fullerene: $[K@Au_{12}Sb_{20}]^{5-}$. *Science* **2023**, *382*, 840–843. [CrossRef] [PubMed]